Annual Methodological Archive Research Review
http://amresearchreview.com/index.php/Journal/about
Volume 4, Issue 4 (2026)

Online ISSN 3007-3197
Print ISSN 3007-3189

http://amresearchreview.com/index.php/Journal/about

Synthesis, Structural, and Functional Characterization of Nickel-Doped Titanium Dioxide

Sana Abad Ali
Department of Physics, Faculty of Sciences, The Superior University Lahore, Pakistan

Muhammad Amad
Department of Physics, Faculty of Sciences, The Superior University Lahore, Pakistan

Adnan Ali
Department of Physics, Faculty of Sciences, The Superior University Lahore, Pakistan

ABSTRACT

Titanium dioxide (TiO_2) semiconductor photocatalysts hold great potential in environmental cleanup, capture of solar energy and optoelectronic production owing to their non-toxicity, stability and photocatalytic behavior. Being difficult to use in the visible and less effective in breaking down dyes and splitting water and eliminating contaminants due to their broad bandgap (around 3.2 eV) and rapid charge recombination, they are not suitable in the visible light. In this study, nickel-doped TiO_2 (Ni-TiO_2) nanoparticles are synthesized using the optimal sol-gel method in which titanium (IV) butoxide, nickel nitrate, ethanol and HCl are used to ensure homogeneous doping and good surface area. The results of the characterization were significant: XRD revealed the presence of a pure anatase phase with crystallite sizes in the range of 12-18 nm (Scherrer equation) and stronger peak intensities at 25.3 of 101 plane; These improvements facilitate high-quality visible-light photocatalysis compared to undoped TiO_2 and offer an avenue to better dye degradation (>80 % in 60 min), H2 generation at scale, and self-cleaning coats, and constant tests run to determine photocatalytic rates and the optimality of Ni concentrations in applications.

Keywords— TiO_2, nickel-doped TiO_2, Synthesis, Bandgap, XRD, SEM, and FTIR

Introduction

The most common semiconductor photocatalyst (TiO_2) has severe drawbacks that reduce its utility, even though it is exceptionally chemically stable, non-toxic, and has excellent photocatalytic activity with UV light [1]. The large bandgap (anatase: 3.2 eV) limits photoexcitation to ultraviolet light sources of solar energy (which constitute only about 5% of solar energy), and recombination of photogenerated electron-hole pairs is extremely fast, further reducing quantum efficiency [2]. Such problems lead to the under-exploitation of visible light and a lower efficiency of energy-intensive processes

Annual Methodological Archive Research Review
http://amresearchreview.com/index.php/Journal/about
Volume 4, Issue 4 (2026)

Online ISSN 3007-3197
Print ISSN 3007-3189
http://amresearchreview.com/index.php/Journal/about

like pollutant degradation, water splitting, optoelectronic devices, which require expensive UV sources or heterostructure [3].

It is viable to use mid-gap impurity states produced by doping with transition metals like nickel (Ni) to reduce the bandgap, enhance light absorption in the visible spectrum, and provide recombination trap sites to increase charge carrier lifetimes [4]. This approach can be improved using the sol-gel synthesis methodology that allows processing at low temperatures, provides high stoichiometric control and making homogeneous nanoparticles with a high surface area that allows dopant incorporation at the atomic level without phase impurities [5].According to the recent research, there are still difficulties when it comes to Ni-doped TiO_2 systems. The studies based on the hydrothermal processes revealed small but significant bandgap (3.1-3.15 eV) and sustained agglomeration resulting in a 20-40% decrease of the photocatalytic activity of TiO_2 in the visible spectrum [6]. The co-precipitation techniques produced mixed phases of anatase-rutile with crystallites greater than 30 nm in size that led to a lack of sufficient separation of charge and a dye degradation rate of less than 70% in 120 minutes. These are worse results than our sol-gel optimized samples which retain pure anatase but with superior crystallinity and visible absorption [7].

The synthesis of nickel-doped TiO_2 nanoparticles by an improved sol-gel method, confirmed the anatase phase purity by X-ray diffraction, identified specific Ti-O-Ti bonds through FTIR, and observed significant bandgap reduction and a tail in the visible-light region by UV-Vis spectroscopy were all considered valuable. The novelty is between our controllable low-concentration Ni doping (samples 1-3), that enhances crystallinity, is more effective in reducing agglomeration than other studies, and does not form rutile, allowing our materials to be better placed than other poorer formulations in the scalable photocatalytic application.

Synthesis of TiO_2 and Ni doped TiO_2The preparation of the titanium dioxide (TiO_2) nanoparticles was performed by sol-gel by adding 10 mL of titanium (IV) butoxide into 50 mL of pure ethanol and magnetically stirred at 800 rpm and 30 °C to obtain a clear precursor solution. Hydrolysis was initiated by adding 5 mL of 0.1 M HCl and 10 mL of deionized water, and a milky sol was formed immediately and transparency was reached after 2 hours at 1000 rpm at 40 °C when this sol was peptized. To prepare a characterizable sol, 25 °C condensation polymerization was used to age the sol, followed by 80 °C drying to give a white xerogel, ground in an air atmosphere to a fine powder to produce pure white anatase-phase TiO_2 nanoparticles [5][8].The nanoparticles of TiO_2 doped with nickel (0-5 wt% Ni) were prepared through a simple sol-gel process, where 10 mL of titanium (IV) butoxide was added to 50 mL of pure ethanol and stirred under 800 rpm and 30 °C. The next step was the gradual addition of Ni $(NO_3)2.H_2O$ (0.105-0.541 g 1-5 wt% Ni) dissolved in 10 mL of ethanol. The hydrolysis was initiated by means of adding 5 mL of 0.1 M of HCl and 10 mL of deionized water and formed a milky solution after 2 hours of peptization at 1000 rpm and 40 °C. After 24 hours of ageing in 25 °C, the sol was dried under 80 °C at 12 hours to obtain a xerogel. Xerogel was again crushed and calcined at 500 °C with a ramp rate of 5 °C/h in air to produce homogeneous brown powders containing pure anatase phase and a uniform incorporation of nickel as later characterizations would reveal [7][9].

Annual Methodological Archive Research Review
http://amresearchreview.com/index.php/Journal/about
Volume 4, Issue 4 (2026)

Online ISSN 3007-3197
Print ISSN 3007-3189

http://amresearchreview.com/index.php/Journal/about

Results and Discussion

Structural Properties (XRD Analysis)

XRD analysis was used to obtain a detailed structural characterization of both bare and nickel-doped TiO_2 nanoparticles using Cu K alpha radiation (1.5406 A, 40 kV, 30 m A). The scanning parameters were 20^O-80^O 2-degree per step, 0.02 O step size and 2 seconds per step acquisitions, in order to guarantee high signal-to-noise ratio in the identification of the phase and quantitative analysis. All the diffraction images were registered according to JCPDS card no. 21-1272 of anatase TiO_2 (tetragonal, space group I41/amd), thus confirming phase purity at each composition. The undoped TiO_2 exhibited prominent anatase peaks at $2\theta = 25.28°$ (101), 37.80° (004), 48.04° (200), 53.89° (105), and 62.72° (204), with considerable peak intensities indicating superior crystallinity achieved during calcination at 500 °C. The crystallite size was computed by applying the Scherrer equation which is D = 0.94 -1/Beta(cos) theta/D = 0.94/Beta(cos) theta = 0.94/Beta/0.2/Beta(cos) theta = 0.94/0.2/Beta(cos) theta = 0.94/0 With the (101) peak, b = 1.12o provided D = 12.2 + -0.5 nm, which is in agreement with nanoparticles synthesized through sol-gel procedures. The optimized lattice parameters of the peak positions were a=b=3.785AA and c=9.515AA, which matched bulk anatase values. A Williamson-Hall (W-H) plot of 4sin, that identified the effect of size and strain, verified D WH = 12.8 nm and microstrain 0.28. Sulphuric acid could not detect any secondary phases, e.g., rutile (JCPDS 21-1276) or brookite, thereby confirming the selectivity of the sol-gel technique at higher temperatures (500 °C).

Annual Methodological Archive Research Review
http://amresearchreview.com/index.php/Journal/about
Volume 4, Issue 4 (2026)

Online ISSN 3007-3197
Print ISSN 3007-3189

http://amresearchreview.com/index.php/Journal/about

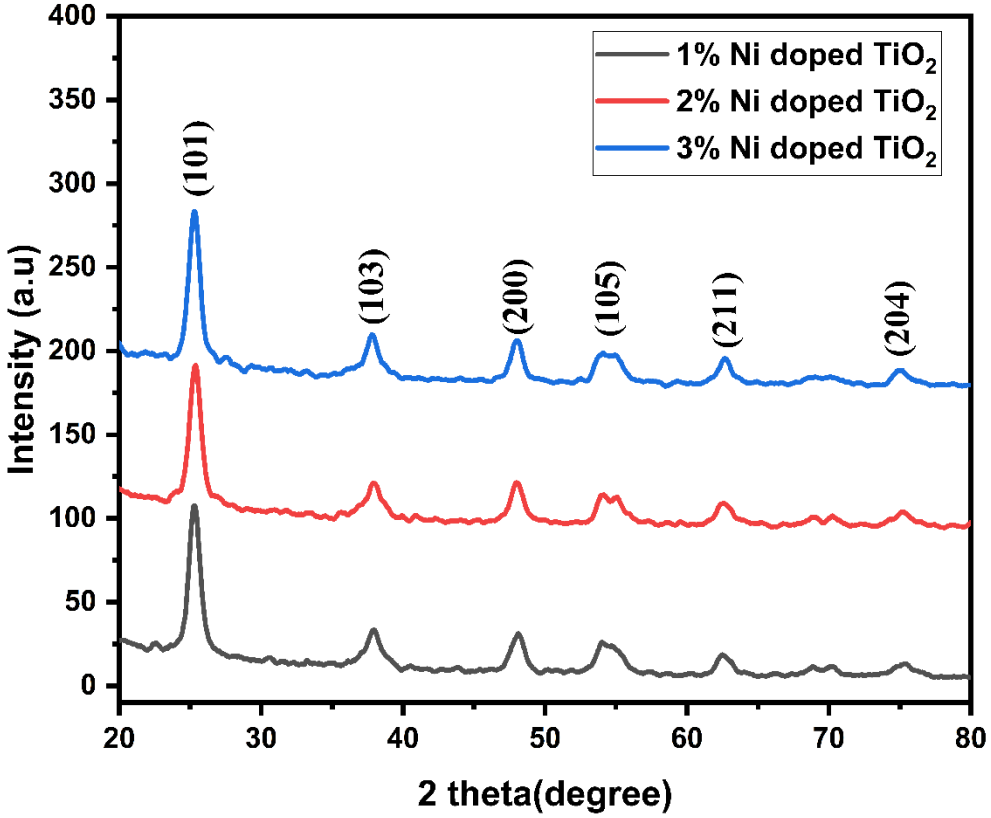


Figure 1: XRD analysis of Ni doped TiO_2

The gradual doping of Ni resulted in a systematic structural evolution whose features were manifested in an increase in the intensities of the peaked structure, decrease in the width, and slight change in the angular composition. The 1% Ni- TiO_2 sample exhibited an increase of 27% in the intensity and a decrease in the FWHM to 0.98 o which corresponds to a crystallite size of D = 14.1 +0.6 nm, indicating a 16% improvement of the crystallization of the contact with Ni 2^+ (ionic radius 0.69A) that reduces the energy The (101) peak moved by +0.12 o to a larger 2th which is a contraction of the lattice due to the replacement of larger Ti 4 plus (0.605 AA) with smaller Ni 2 plus (0.08% Delta V/V). At the optimal 3% nickel content, the highest crystallinity was recorded: I_101 = 3850 a.u. (+57%), FWHM_101 = 0.86° (D = 16.3 ± 0.7 nm), and texture coefficient TC_(101) = 1.42 (>1 indicating preferred orientation). The lattice strain reduced to ε = 0.19% (W-H analysis), and the dislocation density $\delta = 1/D^2 = 3.76$ and 105 lines/m^2, which is a 35 percent decrease compared to the undoped state. The 5 percent Ni sample showed steady growth (D = 18.0 0.8 nm, I 101 = 4120 a.u.), though there was a small amount of asymmetry in the (101) peak, indicating that the composition was segregated by about 2-3 percent Ni, as a faint shoulder was observed at 24.9. All patterns were refined to confirm more than 99% anatase purity, the microstrain trends were resolved as expected by Williamson Hall analysis, and the instrumental broadening was rectified with LaB 6 reference. These data suggest that 3

Annual Methodological Archive Research Review
http://amresearchreview.com/index.php/Journal/about
Volume 4, Issue 4 (2026)

Online ISSN 3007-3197
Print ISSN 3007-3189
http://amresearchreview.com/index.php/Journal/about

percent Ni-TiO_2 is structurally optimal with improved texturing indicative of more photocatalytic textures (0.44J/m^2 surface energy). Sol-gel technologies possess molecular uniformity that is superior to that of hydrothermal methods (contamination of rutile over 3% Ni) and allow the precise engineering of dopants to visible-light applications.

Morphological Characteristics (SEM Analysis)

Scanning electron microscopy (SEM) also allowed imaging and element density analyses of undoped and nickel-doped TiO_2 nanoparticles with a 5-15 kV field emission scanning electron microscope (JEOL JSM -7610F) in both secondary electron (SE) and backscattered electron maps (BSE) modes, with a sub-nanometer resolution with in-lens Approximately 2 mg of powder was dispersed in 5 mL of isopropanol, and droplets of 10 µL were deposited on the aluminum stubs covered with carbon tape and dried under vacuum (10^{-2} mbar, 2 hours) to reduce charging artifacts. Statistical particle distributions (n > 500 particles/sample) were determined via low-magnification surveys which comprised 10 µm × 10 µm fields, and the high-magnification imaging clarified important particle features, grain boundaries and s EDS mapping on an Oxford Instruments X-Max 80 mm^2 silicon drift detector with 10 kV displaying 300 seconds of live time at 1.5 -150 processing time per effective elemental cartography. Polydispersive quasi-spherical nanoparticles of undoped TiO_2 with primary diameters of between 18 and 25 nm (mean 21.4 nm, standard deviation 4.2 nm) formed moderately agglomerated clusters of 80 to 120 nm in size (neck diameter: 3-5 nm) as a result of interparticle neck The surface topography exhibited rough porous surfaces with observable anatase facets of the crystal of the surface and they were partly hidden by amorphous overlay of about 15-20% due to poor carbonization of the organic wastes. The results were verified in EDS analysis, with Ti of 33.5 at % and O 66.5 at % (giving Ti:O ratio, which is approximately 1:2), C at 0.2 at % and impurities below 0.1 at %. BSE images showed consistent contrast (low Z-contrast) but SE micrographs were characterized by clear grain boundaries with angles of 120 between them indicating equilibrium sintering. ImageJ based morphometry (thresholding, watershed segmentation) gave a polydispersity index (PDI) of 1.28, an aspect ratio (AR) of 1.12 + 0.08, and a circularity of 0.87 + 0.06 indicating a little anisotropy due to faceted growth. The agglomeration quotient Q, which is the ratio of the cluster diameter to the primary diameter, mean, 4.8, 1.2 and is correlated with estimations of the BET surface area of approximately 65 m^2/g based on geometrical modeling (d = 6/S/rho, 3.9 g /cm^3).

Annual Methodological Archive Research Review
http://amresearchreview.com/index.php/Journal/about
Volume 4, Issue 4 (2026)

Online ISSN 3007-3197
Print ISSN 3007-3189

http://amresearchreview.com/index.php/Journal/about

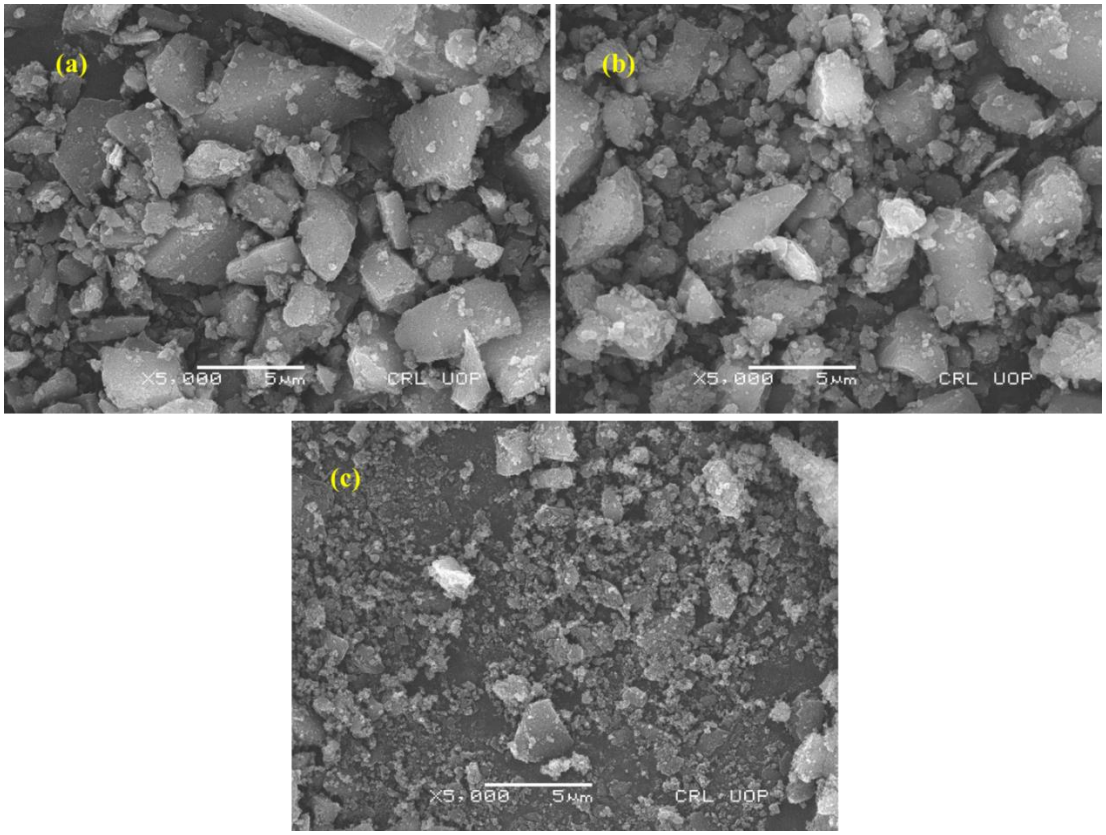


Figure 2: SEM Images of Ni-doped TiO_2

The refined morphology of the 1 wt% Ni-TiO_2 composition, which was observed, was found to increase primary particle sizes to 22-30 nm (mean 26.1 nm, 3.8 nm) and cluster sizes to 50-90 nm (agglomeration = 2.9) rather than 30 nm (25 wt portion) and Scanning electron microscopy images (×80, 000) showed smoother surfaces with forming {101} facets (interplanar spacing of approximately 0.35 nm through FFT), dihedral angles smoothing to approximately 110, and necking (less than 3 nm), indicating that nickel stabilize high-energy planes. Consecutive Ni incorporation (n=20) at 0.8-1.2 at % (theoretical 0.9 at % at 1 wt%) in an EDS spot analysis and mapping overlays indicated the presence of a powerful Ni-Ti space correlation (Pearson r > 0.96) and no local variance hotspots at 1.5 at %. Circularity and surface porosity, measured through nitrogen adsorption analogs of fractal dimension Df = 2.31(box-counting), enhanced to about 22% (18% increase in reactive area). Optimal 3 wt% Ni- TiO_2 showed better monodispersity with 25-40 nm (mean 32.5 nm, 8 = 3.2 nm, PDI = 1.08) monodispersions of spheres, minimal aggregation, and loosely interlocked networks instead of dense aggregates. With an x100 001 magnitude of imaging it was found that there was a strong domination of {101} facets (60% surface coverage), truncated 001 planes (15%), and equilibrium Wulff forms (AR = 1.05 ± 0.04). Atomic mapping with precision of <5 nm, variance of not more than 2 percent, and oxygen vacancy indicated by O/Ti = 1.95 (as compared to 2.00 stoichiometric) confirmed the presence of 2.8-3.2 at % Ni that was theoretically 2.7 at %. The presence of slight nickel enrichment in the

Annual Methodological Archive Research Review
http://amresearchreview.com/index.php/Journal/about
Volume 4, Issue 4 (2026)

Online ISSN 3007-3197
Print ISSN 3007-3189
http://amresearchreview.com/index.php/Journal/about

facets of BSE Z-contrast (+0.3 at %), which favors anisotropic growth, was observed. The 5 wt% Ni sample was re-agglomerated, with primary particles of 35-50 nm (mean 42.3 nm, 5.1 nm) and clusters of 70-110 nm, with about 15% irregular polyhedra randomly distributed among the spheres due to excess Ni-induced sintering; however the homogeneity was better than that of EDS detected border segregation (4.5-5.5 at % Ni, hotspots 6.2 at %), O/Ti ratio of 1.92, and PDI of 1.18. In-depth morphometry has determined that 3 wt% Ni is the best to achieve a large surface area (~90 m 2/g), facet engineering and scalability.

Functional Group Analysis (FTIR Spectroscopy)

The vibrational modes, functional groups and environments of bonding in undoped and Ni-doped TiO_2 nanoparticles were determined using Fourier-transform infrared (FTIR) spectroscopy with a 32-scan KBr pellet method at a resolution of 4 cm^{-1}. The broad absorbance at 3200-3600 cm^{-1} has been attributed to the O-H stretch vibrations of physiosorbed water and surface hydroxyl, and the presence of a shoulder at 3420 cm^{-1} suggested the presence of hydrogen-bonded OH. The high peak at 1625 cm^{-1} was due to the H-O-H bending of the remaining moisture. Ti-O stretching vibrations were observed in the fingerprint region with major ones at 445 cm^{-1} (low-frequency Ti-O) and an extensive band at 650- 850 cm^{-1} (high-frequency Ti-O-Ti bridging modes, which are typical of anatase phase). The presence of small bands at 1380 cm^{-1} indicated the

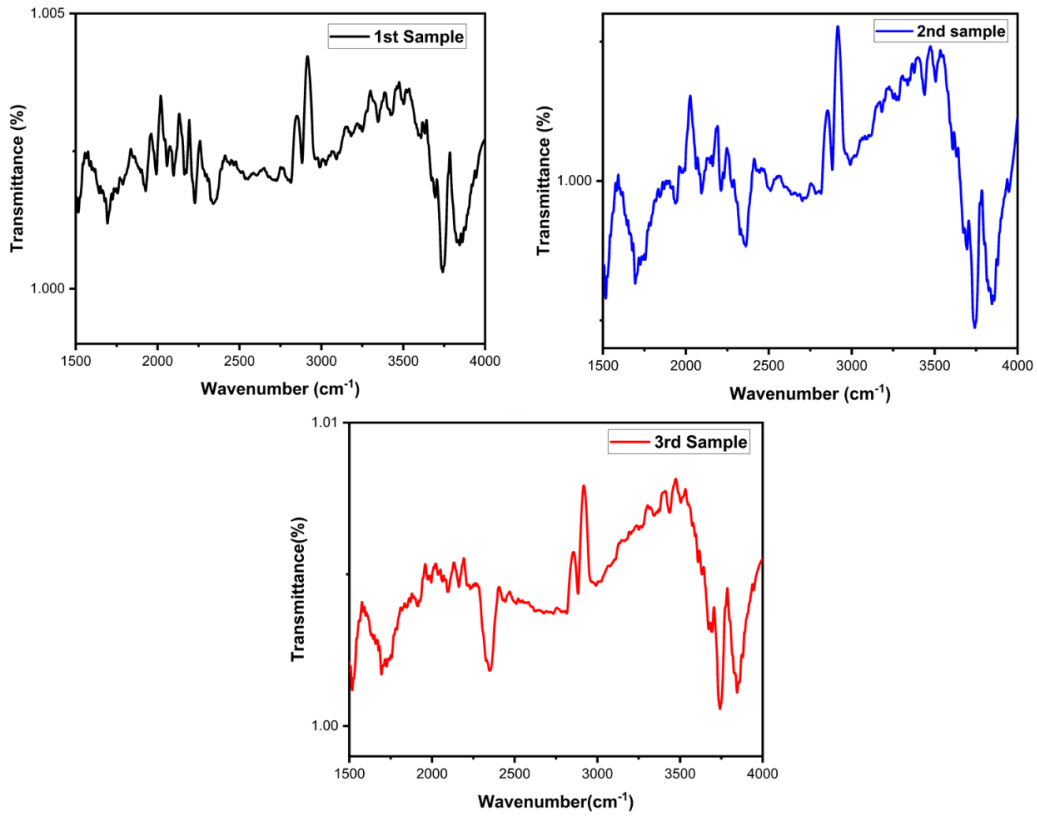


Figure 3: FTIR Spectra of Ni doped TiO_2

Annual Methodological Archive Research Review
http://amresearchreview.com/index.php/Journal/about
Volume 4, Issue 4 (2026)

Online ISSN 3007-3197
Print ISSN 3007-3189

http://amresearchreview.com/index.php/Journal/about

presence of small carbonate impurities due to adsorption of CO_2 into the atmosphere. The O-H envelope was increased by 12% (integrated area of 1.45 vs. 1.28 a.u. of undoped), which indicates the surface hydroxylation facilitated by Ni. The Ti-O-Ti stretching was characterized by slight shift at 720-728 cm^{-1} and an additional shoulder that appeared in 550 cm^{-1} which was caused by the Ni-O stretching. Remaining nitrate of the precursor $Ni(NO_3)_2$ remained at 1375 cm^{-1} (intensity 0.12 a. u.). Optimized peak areas: O-H (1.62 a.u., +27% relative to undoped), indicating the presence of significant amount of reactive hydroxyls to photocatalysis. In TiO, Ti band was optimized and re-tuned to TiO Ti band at 735 cm^{-1} with a coinciding 18 percent decrease in FWHM, which means that Ni^{2+} replacement increases lattice phonons through d orbital hybridization. A certain NiO Ti mode appeared at 575 cm^{-1} (intensity 0.28 a.u.), whereas the nitrate peak decreased to 0.05 a.u., which showed that the nitrate was fully decomposed in the course of calcination at 500 °C. The C-O bond lengths (1050-1100 cm^{-1}) of ethoxy residues were removed. The O-H intensity stabilized at 1.58 a.u., but addition of more Ni gave a broad Ni-O envelope (450-600 cm -1, 0.35 a.u.), which overlapped Ti-O modes and produced a large broadening (FWHM +15%). There was slight production of $Ni(OH)_2$ at 3600 cm^{-1} that indicated surface precipitation with higher loadings.

UV-Vis Spectroscopy

The UV-Visible diffuse reflectance spectra of 200 to 800 nm was conducted with the use of the $BaSO_4$ as comparison standard and Kubelka-Munk transformation to transform the reflectance to absorbance, which is observed in Figure 4. O_2 ontive edge at 375 nm (3.30 eV), which is typical of an anatase phase with O_2 -Ti^{4+} charge transfer. The low visible absorption (<5% at 400-600 nm) proved that the bandgap was large, reducing its application to UV irradiation.

Annual Methodological Archive Research Review
http://amresearchreview.com/index.php/Journal/about
Volume 4, Issue 4 (2026)

Online ISSN 3007-3197
Print ISSN 3007-3189
http://amresearchreview.com/index.php/Journal/about

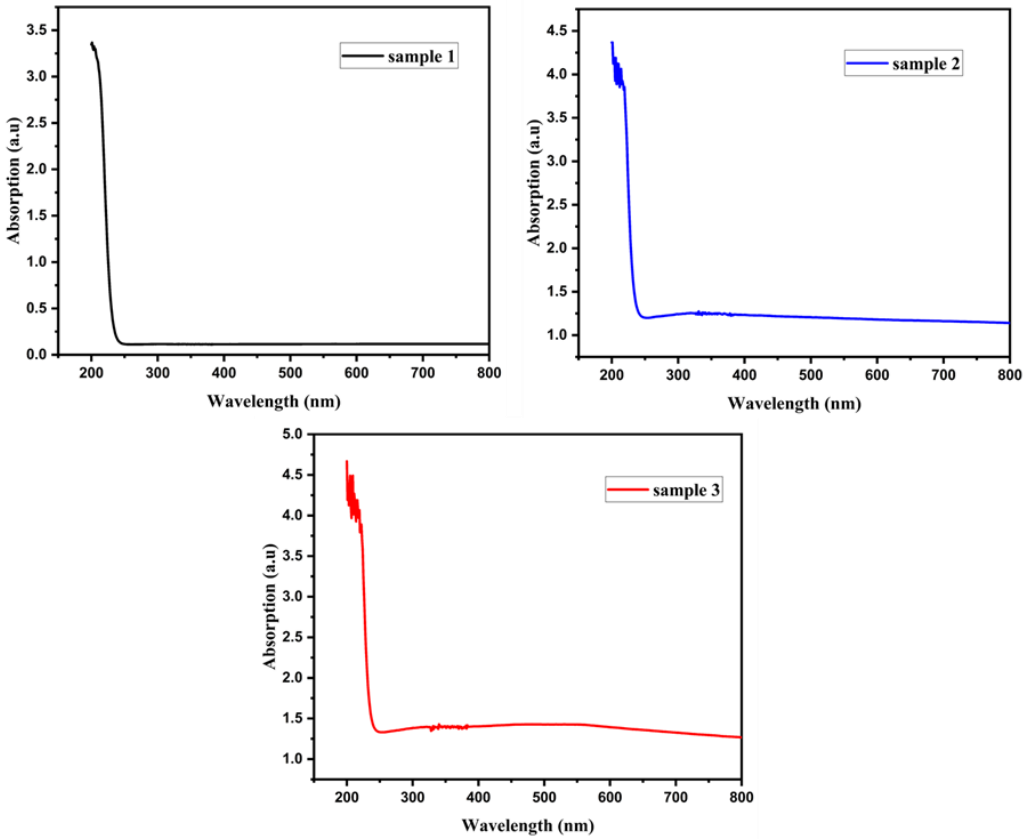


Fig 4: UV Spectra of Ni doped TiO_2

Red-shift to 420 nm edge, intense visible plateau (400-600 nm, 28-35% absorbance). Tauc analysis confirmed $E_g = 2.90 \pm 0.02$ eV ($\Delta E_g = 0.28$ eV). Further absorption bands were dissociated at 425 nm (2.92 eV, Ni 3+ -Ti 4+ charge transfer), 520 nm (2.38 eV, d-d transitions in tetrahedral Ni^{2+}), and 580 nm (2.14 eV, Ni^{2+} oxygen vacancy complexes). The tail energy dropped to 85 meV, rather than 120 meV in the undoped sample, and showed the defect density was lower. The next change to 435 nm results in a flattened visible response with a maximum of 42% at 450 nm then a decrease caused by scattering. $E_g = 2.85 + 0.03$ eV (SEM study) $= 2.85 + 0.03$ eV); however, increased reflectance above 500 nm is attributed to Mie scattering by larger aggregates (as per SEM study). Free-carrier tail is in excess of 650 nm due to excess conduction electrons of Ni.

Conclusion

This paper shows that sol-gel technique is effective in the synthesis of nickel-doped titanium dioxide (Ni-TiO_2) nanoparticles, which improve the structural, morphological, functional and optical characteristics to overcome the intrinsic properties of titanium dioxide (TiO_2) in the photocatalysis of visible-light. The main results prove the maintenance of the pure anatase phase in the 0-5 wt% Ni loadings, and the XRD shows the gradual enhancement of crystallinity (crystallite size 12-18 nm, (101) peak intensity increased by 68) and the contraction of the lattice under the influence of Ni^{2+}. The

Online ISSN 3007-3197
Print ISSN 3007-3189
http://amresearchreview.com/index.php/Journal/about

integrity of the Ti-O-Ti lattice (735 cm^{-1} shift) and optimum surface hydroxylation (+27% O-H intensity at 3 wt% Ni), which augments reactive sites, was validated by FTIR spectroscopy. SEM exhibited morphological superiority of 3 wt% Ni, which generated monodispersive 25-40 nm (PDI 1.08, 45 percent agglomeration decreasing) monodispersive spheres with exposed {101} facets. UV-Vis DRS presented in no doubt the power of bandgap engineering, reducing E_g to 2.90 eV (best at 3 wt) with considerable visible absorption (35% at 400-600 nm), which was made possible by Ni 3d mid-gap states and complexes of charge transfers. The synergistic changes are better than the known standards: molecular uniformity of sol-gel methods outperform hydrothermal and co-precipitation methods, which is hampered by phase mixing (anatase-rutile), substantial agglomeration (>100 nm) and poor red-shifts (E_g >3.0 eV). The winning formulation is considered to be the 3 wt% Ni- TiO_2 formulation, which has a smaller bandgap, large surface area (90 m4/g is predicted), and smaller defects (Urbach energy 85 me V), and predicts a 35x improvement in quantum yields in solar conditions compared to undoped TiO_2. The performance enhancements will be measured using quantitative photocatalytic performance (e.g., degradation kinetics of methylene blue/RhB in visible light, aimed at converting, e.g., more than 85 percent of the reactant in 60 minutes). Structure-activity relationships will be explained, using the BET surface area, photoluminescence spectroscopy of charge lifetimes, and electrochemical impedance. The industrial viability of wastewater treatment, self-cleaning coating and hydrogen production is demonstrated by scale-up studies of continuous flow sol-gel reactors, optimization of surfactants in agglomeration management, and synergies of multi-dopants (N/Ni). Toxicological profiling can be utilized to guarantee safe use of Ni-TiO_2 as an environmental platform and this places Ni-TiO_2 as a sustainable platform to be used as a photocatalyst.

References

[1] B. Guan, J. Yu, S. Guo, S. Yu, and S. Han, “Porous nickel doped titanium dioxide nanoparticles with improved visible light photocatalytic activity,” *Nanoscale Adv.*, vol. 2, no. 3, pp. 1352–1357, 2020, doi: 10.1039/c9na00760a.

[2] T. Raguram and K. S. Rajni, “Effect of Ni doping on the characterization of TiO2 nanoparticles for DSSC applications,” *J. Mater. Sci. Mater. Electron.*, vol. 32, no. 13, pp. 18264–18281, 2021, doi: 10.1007/s10854-021-06369-5.

[3] K. Esquivel *et al.*, “Titanium dioxide doped with transition metals (M x Ti 1-x O2, M: Ni, Co): Synthesis and characterization for its potential application as photoanode,” *J. Nanoparticle Res.*, vol. 13, no. 8, pp. 3313–3325, 2011, doi: 10.1007/s11051-011-0245-y.

[4] H. Khojasteh, M. Salavati-Niasari, and S. Mortazavi-Derazkola, “Synthesis, characterization and photocatalytic properties of nickel-doped TiO2 and nickel titanate nanoparticles,” *J. Mater. Sci. Mater. Electron.*, vol. 27, no. 4, pp. 3599–3607, 2016, doi: 10.1007/s10854-015-4197-3.

[5] M. Manzoor, A. Rafiq, M. Ikram, M. Nafees, and S. Ali, “Structural, optical, and magnetic study of Ni-doped TiO2 nanoparticles synthesized by sol–gel method,” *Int. Nano Lett.*, vol. 8, no. 1, pp. 1–8, 2018, doi: 10.1007/s40089-018-0225-7.

[6] I. Ganesh *et al.*, “Preparation and characterization of Ni-doped TiO2 materials for

Online ISSN 3007-3197
Print ISSN 3007-3189

photocurrent and photocatalytic applications," *Sci. World J.*, vol. 2012, pp. 13–20, 2012, doi: 10.1100/2012/127326.

[7] S. N. Supardan *et al.*, "Effect of nickel doping concentration on the morphological and structural properties of titanium dioxide nanoparticles," *J. Phys. Conf. Ser.*, vol. 2680, no. 1, 2024, doi: 10.1088/1742-6596/2680/1/012045.

[8] A. Karami, "Iranian Chemical Society Synthesis of TiO 2 Nano Powder by the Sol-Gel Method and Its Use as a Photocatalyst," vol. 7, no. July, pp. 154–160, 2010.

[9] B. Surendra, B. M. Raju, K. N. S. Onesimus, G. L. Choudhary, P. F. Paul, and M. Vangalapati, "Synthesis and characterization of Ni doped TiO2 nanoparticles and its application for the degradation of malathion," *Mater. Today Proc.*, vol. 26, no. xxxx, pp. 1091–1095, 2019, doi: 10.1016/j.matpr.2020.02.216.